Modeling the appearance of special effect pigment coatings

Thomas A. Germer and Maria E. Nadal

Optical Technology Division
National Institute of Standards and Technology
Gaithersburg, Maryland 20899

ABSTRACT

Metallic and pearlescent coatings are becoming increasingly important in automotive, currency, and cosmetic applications. These coatings consist of metallic or dielectric platelets suspended in a binder, and are often applied between a pigmented basecoat, and a transparent topcoat. The scattering properties of these composite coatings vary depending upon the incident and viewing directions, as well as the wavelength. The complex nature of the scattering arises from the competition between multiple scattering sources: front surface reflection from the topcoat, reflection from the platelets, diffuse scattering from the pigmented undercoat, and scattering between platelets. The complex interplay between multiple scattering sources affects the ability to achieve quality control during the preparation of these coatings. In addition, the topcoat surface morphology, the properties of the pigmented basecoat, and the intrinsic properties, concentration, and angular distribution of the platelets influence the final appearance of the coating. In this paper, we will present models for light scattering from front surface facet reflection, subsurface flake reflection, and diffuse subsurface scattering. Experimental scattering measurements on pearlescent coatings show that the polarization can be well described in different geometry regimes by these different scattering sources. The models can be used to extract the slope distribution function of the flakes from the intensity data, but some aspects of the results behave inconsistently. Comparison is also made between experimental and calculated diffuse reflectance spectra. These results are intended to enable improved characterization of special effect coatings necessary for quality control and appearance modeling applications.

Keywords: appearance, coatings, colorimetry, metallic, paint, pearlescent, polarization, scattering

1. INTRODUCTION

Special effect pigments provide a broader range of appearance attributes than is available from traditional absorption and scattering pigments.[1] Metallic and pearlescent paints use thin platelets made out of metallic and dielectric materials, respectively. Optically thin coatings applied to the platelets contribute interference effects, which allow the appearance to vary depending upon illumination and viewing conditions. The complexity of the appearance of coatings containing special-effect pigments necessitates an equivalently complicated description of their scattering behavior in order to facilitate process control and characterization. Since objects painted with these coatings, such as automobiles, may have curved surfaces and be viewed from many different directions, this characterization must be sufficiently complete to represent the visual perception of the materials under the range of geometries for which they will be viewed.

A general scattering function can be extremely complicated.[2] Being a function of, amongst other things, the incident direction, the scattering direction, the polarization, and the wavelength, measuring it with sufficient resolution is time-consuming and nearly impossible to perform fully even in a research, let alone a production, environment. However, several assumptions can be made to reduce the number of these parameters. The requirement of reciprocity simplifies the function slightly, reducing the number of measurements by a factor of two. Reducing the dimension of the problem is much more useful; if the material can be assumed to be isotropic, then the number of directional parameters may be reduced from four to three. Understanding the scattering mechanisms, however, can decrease the number of parameters substantially. For example, if one knows that an isotropic material is scattering due to locally-flat surface facets, then one only needs to know (besides the optical constants of the material) the distribution of slopes to completely describe the scattering as a function of geometry and wavelength,[3,4] thereby reducing the dimensionality of the problem to one.

Figure 1 shows a schematic representation of a composite flake-pigment coating. Such a coating can be considered to consist of three basic layers. The deepest layer is a diffusely scattering pigmented layer. Above that is a layer containing flakes whose surface normals are distributed narrowly about the mean surface normal of the sample. Finally, a clear topcoat is applied which has a smooth surface, though it often has a large amount of long wavelength roughness referred to as *orange-peel*. The binding materials for all of the layers are assumed to have indices matched to one another, so that reflections

from the layer interfaces can be ignored. In this simple view of the composite coating, the scattering of light is assumed to arise from three different scattering mechanisms: local specular reflection from the top interface (facet model), specular reflection from the platelets (flake model), and diffuse scattering from the undercoat (diffuse model).
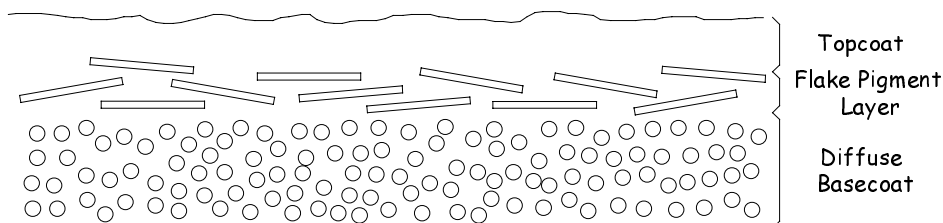
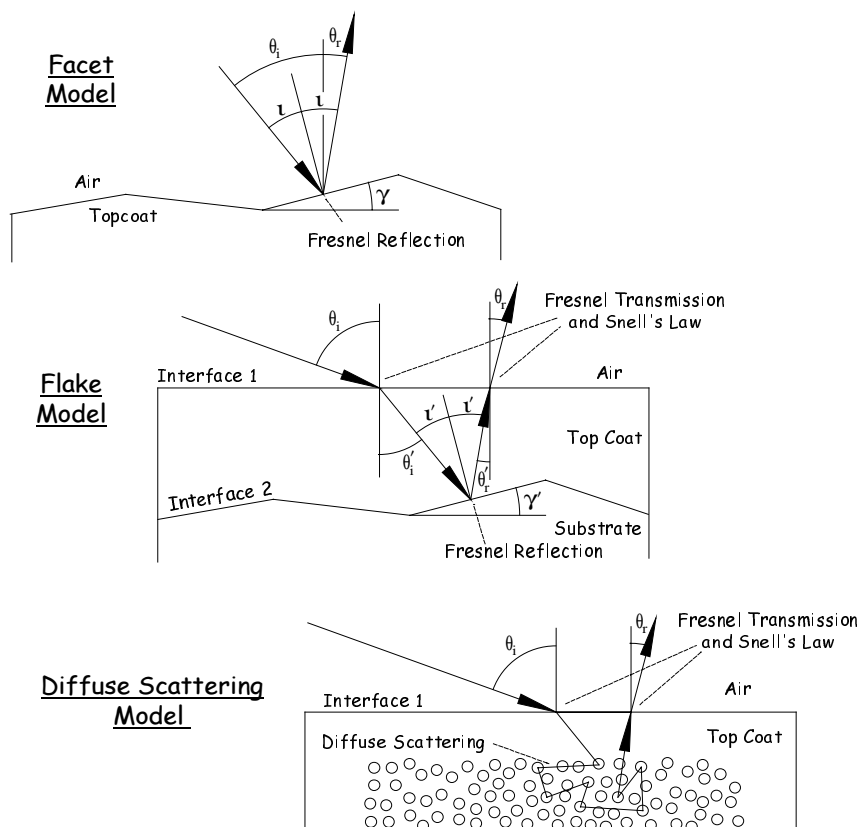**Figure 1.** Schematic diagram illustrating the properties of the paint layer.

Figure 2. Schematic illustrations for three models described in this paper: the facet scattering model (top), the flake or subsurface facet scattering model (middle), and the diffuse scattering model (bottom).

It is the purpose of this paper to present models for light scattering appropriate for special effect pigment coatings, and to investigate the utility of polarized light scattering for separating the various scattering mechanisms. Polarized light scattering has been shown to enable the distinction amongst numerous scattering mechanisms in a number of other systems.[5–11] In many cases, the scattering function is a product of two factors, one of which is dependent upon the source of the scattering, which also determines its polarization properties, and another, which depends upon the statistical description of the ensemble of scatterers and which primarily affects only the intensity distribution. This separation of the scattering function into two functions is analogous to the use of form factors and structure factors, respectively, in x-ray scattering.[12] This effect has been predicted and observed for a number of different scattering mechanisms, including roughness of one[7,10] or more[6] interfaces, particulate contaminants,[8,9] and subsurface defects.[7]

In Section 2, theories for scattering from top surface roughness, subsurface flakes, and subsurface diffusion will be outlined. In Section 3, the measurement procedures employed by this study will be described. In Section 4, the results are presented and discussed. Finally, in Section 5, the results of this study are summarized.

2. THEORY

Light is assumed to be incident on the sample at an angle θ_i from the mean surface normal. The direction of scattered light is parameterized by a polar angle θ_r and an azimuthal angle ϕ_r relative to the flat surface. A right-handed basis set $\{\hat{\mathbf{s}}, \hat{\mathbf{p}}, \hat{\mathbf{k}}\}$ is used to describe the polarization of the light, where $\hat{\mathbf{k}}$ is a unit vector in the direction of propagation, $\hat{\mathbf{s}}$ is a unit vector perpendicular to the plane of incidence (or viewing), and $\hat{\mathbf{p}} = \hat{\mathbf{k}} \times \hat{\mathbf{s}}$ is a unit vector in the plane of incidence (or viewing). There are separate basis sets for the incident and reflected directions, denoted by the subscripts i and r, respectively. Light which is polarized with its electric field along the $\hat{\mathbf{s}}$ ($\hat{\mathbf{p}}$) direction is considered to be s-polarized (p-polarized). In this section, we will discuss light scattering models which are believed to apply to the paint samples studied: scattering from surface facets, subsurface flakes, and diffuse scattering. Computer codes that implement these models have been, or will soon be, made publicly available on the world-wide-web.[13]

2.1. Facet Scattering Model

The scattering from surface roughness in the large amplitude limit is often approached by treating the scattering as specular reflection from aligned facets on the surface. The model is illustrated in Fig. 2(top). Often referred to as specular point theory, and described in detail by Barrick,[3] the model assumes that an observer sees the contributions from those surface facets which are aligned to specularly reflect light from the source towards the observer direction. The facets are assumed to have their slopes ζ distributed randomly according to an isotropic slope distribution function, $S(\zeta)$, defined such that the probability that the magnitude of the slope at a given location (x,y) on the surface is between ζ and $\zeta + d\zeta$ is given by $2\pi\zeta S(\zeta) d\zeta$. The alignment of the facet which specularly reflects from the incident direction to the viewing direction is uniquely determined by the scattering geometry. The cosine of the local incident angle onto a facet, ι, is given by

$$\cos\iota = [(1 - \sin\theta_i \sin\theta_r \cos\phi_r + \cos\theta_i \cos\theta_r)/2]^{1/2} . \tag{1}$$

The facet is tilted from the surface plane by an angle γ, the tangent of which is its slope ζ, and is given by

$$\zeta = \tan\gamma = (\sin^2\theta_i + \sin^2\theta_r - 2\sin\theta_i \sin\theta_r \cos\phi_r)^{1/2} /(\cos\theta_i + \cos\theta_r) . \tag{2}$$

Given the angle-dependent reflection coefficients of the topcoat/air interface, $r_s(\iota)$ and $r_p(\iota)$, the Mueller matrix bidirectional reflectance distribution function (BRDF) for scattering from a distribution of facet angles is given by

$$\mathbf{F}_r^{\text{facet}} = (1 + \zeta^2)^2 S(\zeta)/(4a_1^2 \cos\theta_i \cos\theta_r)\mathbf{M}(\mathbf{q}^{\text{facet}}) \tag{3}$$

where $\mathbf{M}(\mathbf{q}^{\text{facet}})$ is the Mueller matrix derived from the Jones matrix $\mathbf{q}^{\text{facet}}$, which has the elements

$$q_{ss}^{\text{facet}} = r_p(\iota) \sin\theta_i \sin\theta_r \sin^2\phi_r + a_2 a_3 r_s(\iota) , \tag{4a}$$

$$q_{sp}^{\text{facet}} = -\sin\phi_r [a_2 r_s(\iota) \sin\theta_r - a_3 r_p(\iota) \sin\theta_i] , \tag{4b}$$

$$q_{ps}^{\text{facet}} = -\sin\phi_r [a_3 r_s(\iota) \sin\theta_i - a_2 r_p(\iota) \sin\theta_r] , \tag{4c}$$

$$q_{pp}^{\text{facet}} = r_s(\iota) \sin\theta_i \sin\theta_r \sin^2\phi_r + a_2 a_3 r_p(\iota) , \tag{4d}$$

and where

$$a_1 = \sin^2 2\iota , \tag{5a}$$

$$a_2 = \cos\theta_i \sin\theta_r + \sin\theta_i \cos\theta_r \cos\phi_r , \tag{5b}$$

$$a_3 = \sin\theta_i \cos\theta_r + \cos\theta_i \sin\theta_r \cos\phi_r . \tag{5c}$$

In Eqs. (4), the first subscript denotes the incident polarization, while the second denotes the scattered polarization. Note that the existence of any conforming dielectric coating on the surface can be included in the model by using the appropriate reflection coefficients $r_s(\iota)$ and $r_p(\iota)$ calculated for such a coating. The scattering intensity is proportional to the product of the isotropic two-dimensional slope distribution function, $S(\zeta)$, and other factors, which depend only upon the geometry and op-

tical constants of the materials. The polarization of the scattered light, within this approximation, is also independent of the function $S(\zeta)$.

The facet model does not account for light which is reflected from the source into the surface plane. These rays are generally expected to undergo further reflections from and transmission into the material, and are usually assumed to contribute to depolarization and a Lambertian background. Extensions of this model attempt to account for surface shadowing by adding shadow functions appropriate for V-grooves[14] or Gaussian roughness.[15] Since the tangent plane approximation assumes local facet scattering in order to enforce boundary conditions, some wave scattering theories, such as vector Kirchhoff theory, tend to predict the same polarization behavior as the facet scattering model.[16,17]

2.2. Flake Scattering Model

Scattering from flakes beneath the surface, or a rough surface under a thick smooth dielectric layer, can be treated in a similar fashion as the facet scattering model, except that one must take refraction into and out of the topcoat and binder into account. Figure 2(middle) shows a schematic of the scattering mechanism. From Snell's law, the sine of the internal angles of the incident and scattered rays are given by

$$\sin \theta_j' = (1/n) \sin \theta_j , \tag{6}$$

where j = i or r, and n is the optical constant of the dielectric layer. By analogy to Eqs. (1) and (2), the local incident angle onto a facet, ι', has its cosine given by

$$\cos \iota' = [(1 - \sin \theta_i' \sin \theta_r' \cos \phi_r + \cos \theta_i' \cos \theta_r')/2]^{1/2} , \tag{7}$$

and a facet which reflects a ray from the incident direction to the scattering direction is tilted from the surface plane by an angle γ', the tangent of which is its slope

$$\zeta' = \tan \gamma' = (\sin^2 \theta_i' + \sin^2 \theta_r' - 2 \sin \theta_i' \sin \theta_r' \cos \phi_r)^{1/2} /(\cos \theta_i' + \cos \theta_r') . \tag{8}$$

The transmission coefficients into the topcoat are given by $t_s(\theta)$ and $t_p(\theta)$ and depend upon n and the properties of any dielectric coatings on the first interface. The Mueller matrix BRDF can then be expressed as

$$\mathbf{F}_r^{\text{flake}} = (1 + \zeta'^2)^2 S'(\zeta') n^2 /[4(a_1')^2 \cos \theta_i \cos \theta_r] \mathbf{M}(\mathbf{q}^{\text{flake}}) \tag{9}$$

where the scattering matrix $\mathbf{q}^{\text{flake}}$ has elements given by

$$q_{ss}^{\text{flake}} = t_s(\theta_i) t_s(\theta_r)[r_p'(\iota') \sin \theta_i' \sin \theta_r' \sin^2 \phi_r + a_2' a_3' r_s'(\iota')] \tag{10a}$$

$$q_{sp}^{\text{flake}} = -t_s(\theta_i) t_p(\theta_r) \sin \phi_r [a_2' r_s'(\iota') \sin \theta_r' - a_3' r_p'(\iota') \sin \theta_i'] \tag{10b}$$

$$q_{ps}^{\text{flake}} = -t_p(\theta_i) t_s(\theta_r) \sin \phi_r [a_3' r_s'(\iota') \sin \theta_i' - a_2' r_p'(\iota') \sin \theta_r'] \tag{10c}$$

$$q_{pp}^{\text{flake}} = t_p(\theta_i) t_p(\theta_r)[r_s'(\iota') \sin \theta_i' \sin \theta_r' \sin^2 \phi_r + a_2' a_3' r_p'(\iota')] \tag{10d}$$

and where

$$a_1' = \sin^2 2\iota' \tag{11a}$$

$$a_2' = \cos \theta_i' \sin \theta_r' + \sin \theta_i' \cos \theta_r' \cos \phi_r \tag{11b}$$

$$a_3' = \sin \theta_i' \cos \theta_r' + \cos \theta_i' \sin \theta_r' \cos \phi_r \tag{11c}$$

The coefficients $r_s'(\iota')$ and $r_p'(\iota')$ are those appropriate for reflection from the binder/flake interface and may include the effects of any dielectric layers deposited onto the flakes. As for the facet scattering model, the flake scattering model does not account for shadowing, large angle reflections, or multiple scattering, but the models can be extended to include these effects. Furthermore, the flake scattering model does not account for light paths which transmit through one or more flakes before being reflected by another flake. The slope distribution function $S'(\zeta')$ quantifies the distribution of flake slopes, as was defined above for the facet scattering model.

Pearlescent pigments consist of a high refractive index (H) material (such as α-Fe_2O_3) coated onto flakes of a lower index (L) material (such as mica).[1] Therefore, we treat the second interface in Fig. 2(middle) as a three layer (HLH) stack on top of the binder material. Since the thicknesses of the flakes have a broad distribution, we further average over the thickness of the lower index material (mica). The thickness of the high index layer is assumed to be uniform.

2.3. Diffuse Scattering Model

The diffuse scattering model is conceptually very simple, and is schematically illustrated in Fig. 2(bottom). Transmission, with transmittances $T_s(\theta_i)$ and $T_p(\theta_i)$, occurs when light strikes the material interface. That light which transmits into the material undergoes multiple scattering events and becomes completely depolarized. Finally, transmission, with transmittances $T_s(\theta_r)$ and $T_p(\theta_r)$, occurs as light leaves the material. While this mechanism strongly depolarizes the light, a small amount of residual polarization occurs due to the differences between the transmission coefficients for s and p polarization. It is straightforward to show that the Mueller matrix BRDF for this scattering model is given by

$$
\mathbf{F}_r^{\text{Diffuse}} = \frac{\alpha}{4\pi}\begin{pmatrix} f_{r0,0}^{\text{Diffuse}} & f_{r0,1}^{\text{Diffuse}} & 0 & 0 \\ f_{r1,0}^{\text{Diffuse}} & f_{r1,1}^{\text{Diffuse}} & 0 & 0 \\ 0 & 0 & 0 & 0 \\ 0 & 0 & 0 & 0 \end{pmatrix},
\tag{12}
$$

where

$$
f_{r0,0}^{\text{Diffuse}} = \left[T_p(\theta_i) + T_s(\theta_i)\right]\left[T_p(\theta_r) + T_s(\theta_r)\right],
\tag{13a}
$$

$$
f_{r0,1}^{\text{Diffuse}} = \left[T_s(\theta_i) - T_p(\theta_i)\right]\left[T_p(\theta_r) + T_s(\theta_r)\right],
\tag{13b}
$$

$$
f_{r1,0}^{\text{Diffuse}} = \left[T_p(\theta_i) + T_s(\theta_i)\right]\left[T_s(\theta_r) - T_p(\theta_r)\right],
\tag{13c}
$$

$$
f_{r1,1}^{\text{Diffuse}} = \left[T_p(\theta_i) - T_s(\theta_i)\right]\left[T_p(\theta_r) - T_s(\theta_r)\right],
\tag{13d}
$$

and α is a constant, which is the reflectance of the diffuse scattering material, not accounting for the interfaces.

3. EXPERIMENT

3.1. Polarized and Spectrophotometric Scattering Measurements

Measurements were performed using two angle-resolved scattering instruments at NIST, the Goniometric Optical Scatter Instrument (GOSI)[18–20] and the Spectral Tri-function Automated Reference Reflectometer (STARR).[21] GOSI is a laser-based system having a high angular resolution, wide dynamic range, full polarimetric capabilities, and the ability to measure scattering out of the plane of incidence. STARR has a continuously-tunable lamp- and monochromator-based illumination source, a lower directional resolution, a lower dynamic range, and can only investigate scattering in the plane of incidence. The tunable-source capabilities of STARR make it more amenable to visual appearance measurements, while the laser-based and polarimetric GOSI enables scattered light measurements from smooth, low scatter, surfaces. The coherent source and high angular resolution of GOSI also creates a large amount of speckle noise in intensity data, which leads to a lower uncertainty in data measured by STARR.

Measurements performed for this study by GOSI used a HeNe laser ($\lambda = 632.8$ nm) and were carried out in two different geometry-scanning modes: in-plane and out-of-plane. The in-plane measurements were carried out with fixed incident angle ($\theta_i = 45°$ or $60°$), scanning the scattering angle in the plane of incidence. The out-of-plane measurements were carried out by fixing the incident and scattering polar angles ($\theta_i = \theta_r = 45°$ or $60°$), while scanning the azimuthal scattering angle ϕ_r from $0°$ to near $180°$. While the instrument is capable of full Mueller matrix measurements, only measurements of the Stokes vector were performed, using specific incident polarizations which are found to yield a high degree of discrimination between scattering sources. In the plane of incidence, such discrimination was obtained by letting the incident light be linearly polarized at $45°$. For out-of-plane measurements, the incident polarization was continuously varied from $45°$ (p+s) at $\phi_r = 0$, to

90° (p) at $\phi_r = 90°$, and to 135° (p–s) at $\phi_r = 180°$. This incident polarization scheme improves the discrimination between the different scattering mechanisms for all ϕ_r, compared to that using a fixed incident polarization state.[5]

The intensity and polarization of the scattered light is characterized by the bidirectional reflectance distribution function (BRDF), f_r, the principal angle of the polarization, η (measured counterclockwise from s-polarization when looking into the direction of propagation), the degree of circular polarization, P_C, and the total degree of polarization, P. The sign of P_C is chosen to be positive for left-circularly polarized light. These parameters can be obtained from the Stokes parameters. While use of the linear Stokes parameters simplifies many calculations, presentation of data with the parameters η, P_C, and P often simplifies interpretation. In particular, η and P_C parameterizes the polarization state of the polarized part of the beam, while P characterizes the unpolarized part. Furthermore, for many scattering mechanisms and experimental geometries, P_C is close to zero, so that η alone distinguishes amongst dominant scattering mechanisms.

Measurements using STARR were performed for incident angles of $\theta_i = 15°$, 45°, and 65°, scanning the scattering angle from $\theta_r = -75°$ to 75° in 5° increments, and scanning the incident wavelength from 380 nm to 780 nm in 10 nm incements. The source bandwidth of STARR is 15 nm, and the incident light was linearly polarized at 45°.

3.2. Sample Preparation

The samples consisted of red pearlescent pigments coated onto a diffuse white or black basecoat with a clear topcoat. The black basecoat was chosen to isolate the scattering of the pearlescent flakes from other scattering sources. A white basecoat was chosen to study the effect that a diffusely scattering source contributes to the scattering behavior, and to investigate if the scattering from the basecoat can be separated from the scattering from the special-effect pigment. The samples are identified in this article by Xn, where X signifies either W (for white) or B (black), and n signifies the number of applications of pearlescent pigments. A single application of the pearlescent pigments simulated a dilute layer of such pigments, while four applications was sufficiently dense to mask most of the underlying basecoat. The pigment (Engelhard[22] 459Z) consisted of approximately 90 nm α-Fe_2O_3 (hematite) layers coated onto mica platelets having a median size of 18 µm and thicknesses ranging from 300 nm to 400 nm. The mica platelets have a substantial amount of surface roughness.

4. RESULTS AND DISCUSSION

Figure 3 shows polarimetric data[23] for four samples (B1 and B4 on the left, and W1 and W4 on the right) measured using GOSI in the plane of incidence with $\theta_i = 60°$. The interpretation of data measured for $\theta_i = 45°$ and for data measured out of the plane of incidence were consistent with that shown in Fig. 3. Furthermore, the samples having two and three applied coatings of the pearlescent pigments had results ranging between those having one and four applications, as expected. Theoretical calculations, using the models described in Sec. 2.2, accounting for the distribution of mica thicknesses, are included in Fig. 3.

For all of the samples, the BRDF is highly peaked in the specular direction (θ_r near 60°), and the measured value of the BRDF in this regime is limited by the 1.39×10^{-4} sr collection solid angle used for these measurements. For all of the samples shown, the polarimetric values η, P_C, and P match the theoretical prediction of the facet model, as one would expect for front surface reflection. In particular, the total degree of polarization P is very close to unity. Away from the specular direction and for all but the largest scattering angles, the BRDF measured for samples W4 and B4 are similar, suggesting that scattering from the pearlescent pigment dominates the scatter, as one would expect from a saturated and nearly completely covering paint layer. Likewise, the polarimetric signatures of samples W4 and B4 are very similar. As expected, the BRDF from sample B1 is lower than that from B4 due to the lower concentration of flakes, and the BRDF of sample W1 is higher and flatter than W4 due to an increased contribution from the white undercoat layer. The polarization parameters describing the polarized part of the light (η and P_C) are consistent with the model for subsurface flake scattering. The total degree of polarization is fairly low, decreasing with number of flake applications for the black sample and increasing with the number of applications of flakes for the white sample. Presumably, multiple scattering contributes to depolarization, and increasing the concentration of flakes increases the amount of depolarization, but the saturated amount of depolarization from the flakes never achieves the degree of depolarization obtained from the diffuse scattering of the white basecoat.

An interesting behavior can be observed in the regime near, but not at, the specular direction. In this regime, two weakly depolarizing scattering sources, the front surface facet scattering and the subsurface flake scattering, contribute at comparable

levels to the net scattering, but the sources are incoherent with each other. The effect of this mechanistic competition can be seen in Fig. 3 as dips in the total degree of polarization P on both sides of the specular direction.

Lastly, at the very largest scattering angles shown for samples W1 and W4, the values for η deviate significantly from the flake scattering model. At these scattering angles, the basecoat is still visible through the pearlescent flake layer, contributing significantly to depolarization and pushing the results for η towards that predicted by the diffuse scattering model (p polarization, or $\eta = 90°$).
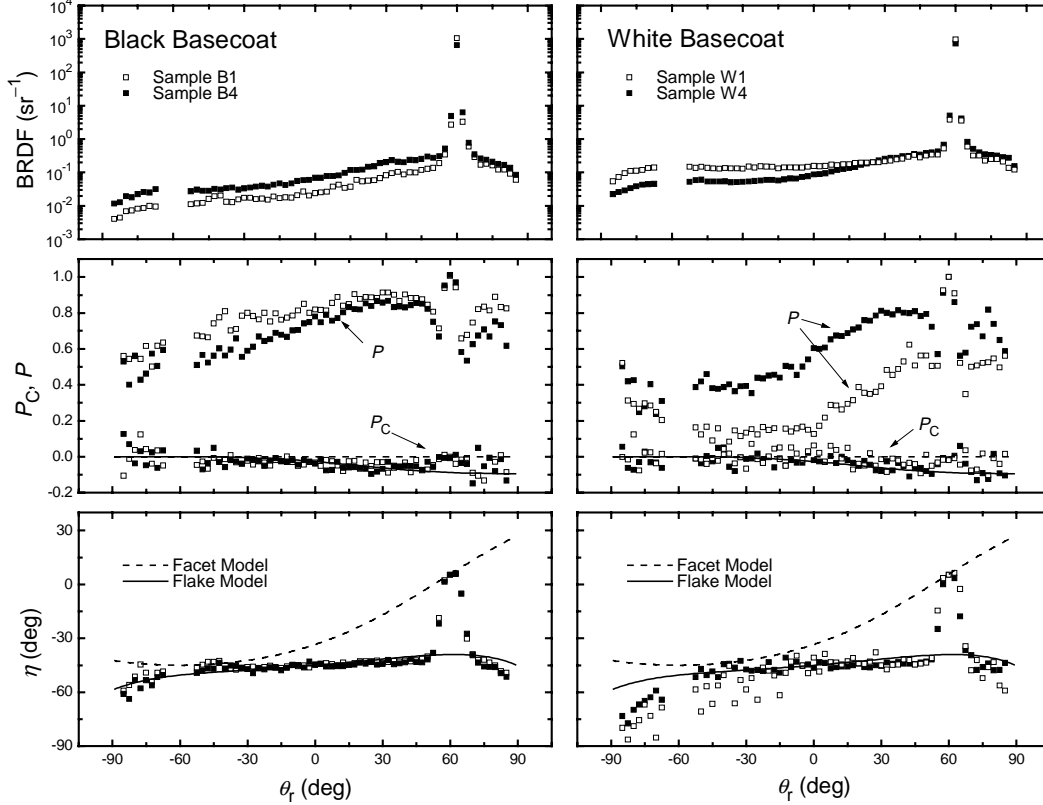
Figure 3. The BRDF (top), degrees of polarization (P and P_C, middle), and principal angle of polarization (η, bottom) for pearlescent pigments applied to the black basecoat samples (B1 and B4, left) and the white basecoat samples (W1 and W4, right) measured in the plane of incidence. The light was incident at an angle $\theta_i = 60°$, was linearly polarized 45° from the plane of incidence, and had a wavelength of 632.8 nm. The theoretical predictions of the facet scattering model applied to the topmost interface (dashed curve) and the flake scattering model applied to the pearlescent flakes (solid curves) are shown for the polarization parameters.

According to Eq. (9), the scattered intensity resulting from subsurface flakes should be proportional to the probability distribution function of slopes, $S'(\zeta')$. Therefore, it is straightforward to convert the measured BRDF to $S'(\zeta')$. Figure 4 shows the results of this analysis applied to samples B1 and B4, using only the polarized part of the measured light (that is using $P f_r$). Included in Fig. 4 are data from in-plane measurements (both forward scattering and backward scattering) and out-of-plane measurements using GOSI with 632 nm light, and in-plane measurements using STARR with 640 nm light. The results for the sample with the most dilute concentration of flakes, sample B1, show the distribution function following a single smooth curve, demonstrating that the flake scattering model describes the scaling law which unifies all of the data. These data yield a straight line when plotted on a semi-logarithmic graph, further simplifying the parameterization of the data. That is, the results for sample B1 are consistent with scattering from flakes having an exponential slope distribution function, characterized by a 1/e slope of approximately 0.15 (rms slope of 0.4).

The results for sample B4, shown in Fig. 4, are not as consistent with flake scattering as those for sample B1. While the polarization parameters agree very well with the flake scattering model, the slope distribution function shown in Fig. 4 does not follow a single curve. In fact, the out-of-plane data and the in-plane forward scattering data ($\theta_r > \theta_i$), all follow along the lower curve, while the in-plane backward scattering data ($\theta_r < \theta_i$) all follow the upper curve. Including all of the scattered light (f_r vs $P f_r$) in the analysis does not change the qualitative interpretation of the data for sample B4 in Fig. 4. This finding

might suggest that multiple scattering between flakes, which is not accounted for in the model, preferentially adds intensity towards the surface normal. While the degree of polarization P often indicates the degree to which multiple scattering occurs, multiple scattering does not necessarily contribute to depolarization. Therefore, we speculate that multiple scattering from the flakes is contributing to increased intensity towards the surface normal. Such multiple scattering may include both reflection-reflection scattering events, and transmission-reflection scattering events. Since the pearlescent pigments are inherently partially transmitting, the flakes which exist beneath other flakes will contribute to the scattered light. The flake scattering model does not account for multiple flake scattering.
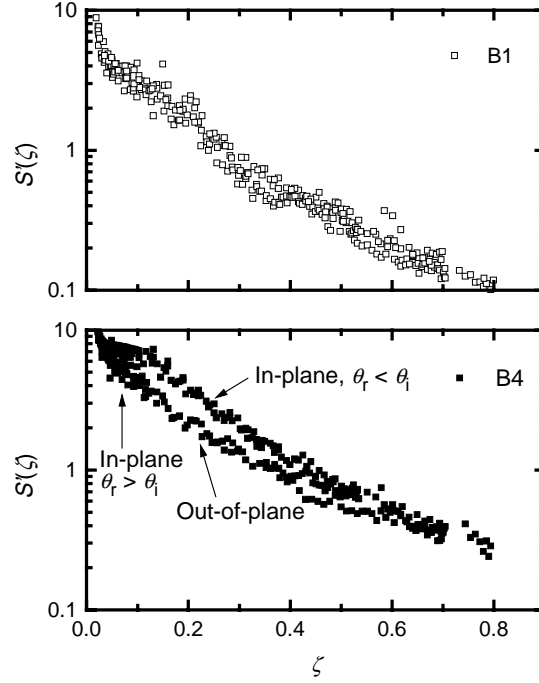

Figure 4. Pearlescent flake slope distribution functions extracted from the data for samples B1 and B4. The analysis was performed using in-plane and out-of-plane data and three incident angles.
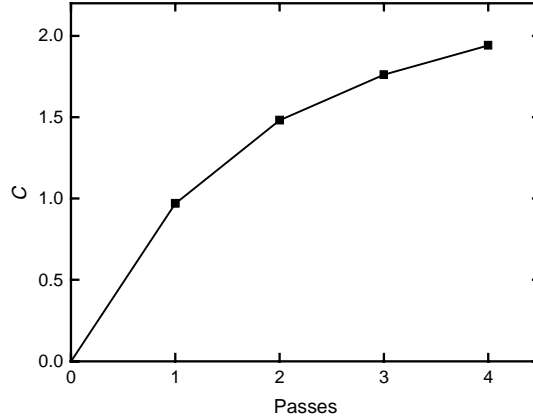

Figure 5. The integral of the facet slope distribution function, C, as a function of the number of applied pearlescent coats, extracted from the light scattering data for samples B1—B4. The point at zero passes was not measured, but was assumed.

The consistency of the distribution function can be checked by determining its normalization; that is,

$$C = \int_0^\infty 2\pi\zeta'\, S'(\zeta')\, \mathrm{d}\zeta' \tag{14}$$

Within the approximations of the flake scattering model, the value C should correspond to the fraction of the surface area which is covered by flakes and should be less than unity. Figure 5 shows the results of this analysis as a function of the

number of pearlescent coatings applied to the black undercoated sample. The value of C grows with the number of coats, reaching a value close to 2. This value may be higher than 1 due to multiple scattering events as described above. Also, the results that one obtains for C depends strongly on the optical constant and thickness used for the α-Fe_2O_3 layer, and the distribution of mica thicknesses.

The scattering models described above in Sec. 2 also allow a calculation of the scattering spectrum. Figure 6 shows a spectrum of sample B1 measured by STARR with $\theta_i = 65°$ and $\theta_r = 0°$, compared to a calculation using the flake scattering model. The spectrum obtained by the model depends very strongly on the optical properties of the flake materials and their thicknesses. Several reasons may account for this lack of agreement, which include insufficient knowledge of the optical constants of the α-Fe_2O_3 layers, insufficient modeling of the roughness of the mica flakes, and the effects of multiple scattering. While gross features of the spectrum are reproduced—location of the maximum near 725 nm, the absorption edge near 575 nm, and the rise in the scattering for short wavelengths—the agreement is insufficient to perform an accurate prediction of color and its change with geometry.
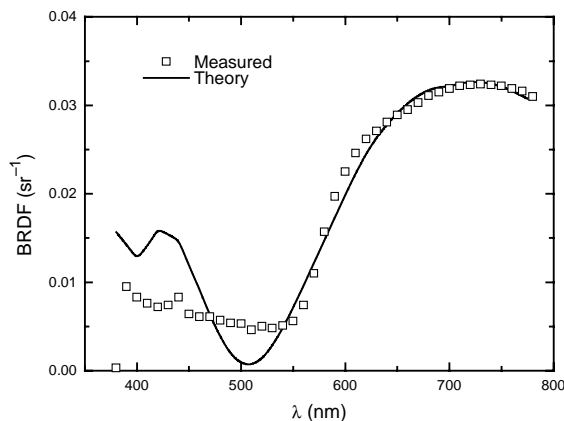

Figure 6. Spectral BRDF measured with $\theta_i = -65°$ and $\theta_r = 0°$ (squares), and the prediction of the flake scattering model (solid curve).

5. SUMMARY AND FUTURE WORK

We have presented models for light scattering, which are appropriate for describing the scattering from pearlescent flake coatings. At small scattering angles, a front surface facet scattering model describes the data. Front surface scattering yields way to subsurface flake scattering at larger scattering angles. At the largest scattering angles, the scatter from the undercoat contributes to the scatter distribution if it is not absorbing. The models work very well for predicting the polarization state of the light and the scaling behavior for different scattering geometries. The polarization state of the scattered light can therefore be used to evaluate the dominant scatter mechanisms acting in different geometries. While the models allow the slope distribution function to be extracted from the data, that slope distribution function does not show the appropriate normalization. Furthermore, the spectrum is not reproduced well by the model. Thus, the models need further refinement before they can be applied to predicting the BRDF of the scattered light. Measurements are currently underway using metallic flake pigments and non-absorbing pearlescent pigments. Metallic flake pigments do not transmit light, so the effects from multiple scattering should be reduced. The use of non-absorbing pearlescent pigments will reduce those uncertainties in the model which result from uncertainties in the material optical properties.

ACKNOWLEDGMENTS

REFERENCES AND NOTES

1. G. Pfaff and P. Reynders, "Angle-dependent optical effects deriving from submicron structures of films and pigments," Chem. Rev. **99,** 1963–1981 (1999).
2. J. C. Stover, *Optical Scattering: Measurement and Analysis*, (SPIE Optical Engineering Press, Bellingham, WA, 1995).
3. D. E. Barrick, "Rough surface scattering based on the specular point theory," IEEE Trans. Ant. Prop **AP-16,** 449–454 (1968).
4. M. E. McKnight, T. V. Vorburger, E. Marx, M. E. Nadal, P. Y. Barnes, and M. A. Galler, "Measurements and predictions of light scattering from clear coatings," Appl. Opt. **40,** 2159–2168 (2001).
5. T. A. Germer, "Polarized light scattering by microroughness and small defects in dielectric layers," J. Opt. Soc. Am. A **18,** 1279–1288 (2001).
6. T. A. Germer, "Measurement of roughness of two interfaces of a dielectric film by scattering ellipsometry," Phys. Rev. Lett. **85,** 349–352 (2000).
7. T. A. Germer and C. C. Asmail, "Polarization of light scattered by microrough surfaces and subsurface defects," J. Opt. Soc. Am. A **16,** 1326–1332 (1999).
8. L. Sung, G. W. Mulholland, and T. A. Germer, "Polarization of light scattered by spheres on a dielectric film," in *Rough Surface Scattering and Contamination,* P.-T. Chen, Z.-H. Gu, and A.A. Maradudin, Eds., Proc. SPIE, **3784**, 296–303 (1999).
9. L. Sung, G. W. Mulholland, and T. A. Germer, "Polarized light-scattering measurements of dielectric spheres upon a silicon surface," Opt. Lett. **24,** 866–868 (1999).
10. T. A. Germer, C. C. Asmail, and B. W. Scheer, "Polarization of out-of-plane scattering from microrough silicon," Opt. Lett. **22,** 1284–1286 (1997).
11. T. A. Germer, "Angular dependence and polarization of out-of-plane optical scattering from particulate contamination, subsurface defects, and surface microroughness," Appl. Opt. **36,** 8798–8805 (1997).
12. N. W. Ashcroft and N. D. Mermin, *Solid State Physics*, (Saunders College, Philadelphia, 1976).
13. T. A. Germer, *SCATMECH: Polarized Light Scattering C++ Class Library* (http://physics.nist.gov/scatmech, 2000).
14. K. E. Torrance and E. M. Sparrow, "Theory of off-specular reflection from roughened surfaces," J. Opt. Soc. Am. **57,** 1105–1114 (1967).
15. B. G. Smith, "Geometrical Shadowing of a Random Rough Surface," IEEE Trans. Ant. Prop **AP-15,** 668–671 (1967).
16. P. Beckmann and A. Spizzichino, *The Scattering of Electromagnetic Waves from Rough Surfaces*, (Pergamon, Oxford, 1963).
17. X. D. He, K. E. Torrance, F. X. Sillion, and D. P. Greenbert, "A comprehensive physical model for light reflection," Computer Graphics **25,** 175–186 (1991).
18. C. C. Asmail, C. L. Cromer, J. E. Proctor, and J. J. Hsia, "Instrumentation at the National Institute of Standards and Technology for bidirectional reflectance distribution function (BRDF) measurements," in *Stray Radiation in Optical Systems III,* R. P. Breault, Ed., Proc. SPIE, **2260**, 52–61 (1994).
19. T. A. Germer and C. C. Asmail, "Goniometric optical scatter instrument for out-of-plane ellipsometry measurements," Rev. Sci. Instr. **70,** 3688–3695 (1999).
20. T. A. Germer and C. C. Asmail, "A goniometric optical scatter instrument for bidirectional reflectance distribution function measurements with out -of-plane and polarimetry capabilities," in *Scattering and Surface Roughness,* Z.-H. Gu and A. A. Maradudin, Eds., Proc. SPIE, **3141**, 220–231 (1997).
21. J. E. Proctor and P. Y. Barnes, "NIST High Accuracy Reference Reflectometer-Spectrophotometer," J. Res. Natl. Inst. Stand. Technol. **101,** 619–627 (1996).
22. Certain commercial equipment, instruments, or materials are identified in this paper in order to specify the experimental procedure adequately. Such identification is not intended to imply recommendation or endorsement by the National Institute of Standards and Technology, nor is it intended to imply that the materials or equipment identified are necessarily the best available for the purpose.
23. The uncertainties in the measured data are less than the sizes of the symbols used for their presentation or the observable point-to-point variations in their values, whichever is larger. Results which depend upon models for their interpretation have no specified uncertainties, because the theoretical models are approximations whose accuracy cannot be quantified.